BIOLOGICAL CRYSTALLOGRAPHY

ISSN 1399-0047

Structures of yeast peroxisomal Δ^3,Δ^2-enoyl-CoA isomerase complexed with acyl-CoA substrate analogues: the importance of hydrogen-bond networks for the reactivity of the catalytic base and the oxyanion hole

Received 2 June 2015
Accepted 19 August 2015

Edited by Z. Dauter, Argonne National Laboratory, USA

Keywords: enoyl-CoA isomerase; crotonase; oxyanion hole; β-oxidation; hydrogen-bond network.

PDB references: yeast Δ^3,Δ^2-enoyl-CoA isomerase, complex with acetoacetyl-CoA, 4zdb; complex with octanoyl-CoA, 4zdc; bound to sulfate ion, 4zdd; F268A mutant, 4zde; helix 10 deletion mutant, 4zdf

Supporting information: this article has supporting information at journals.iucr.org/d

Goodluck U. Onwukwe,[a] M. Kristian Koski,[a] Petri Pihko,[b] Werner Schmitz[c] and Rik K. Wierenga[a]*

[a]Biocenter Oulu and Faculty of Biochemistry and Molecular Medicine, University of Oulu, Oulu, Finland, [b]Department of Chemistry, University of Jyväskylä, Jyväskylä, Finland, and [c]Department of Biochemistry and Molecular Biology, University of Würzburg, Biozentrum, Am Hubland, 97074 Würzburg, Germany. *Correspondence e-mail: rik.wierenga@oulu.fi

Δ^3,Δ^2-Enoyl-CoA isomerases (ECIs) catalyze the shift of a double bond from 3*Z*- or 3*E*-enoyl-CoA to 2*E*-enoyl-CoA. ECIs are members of the crotonase superfamily. The crotonase framework is used by many enzymes to catalyze a wide range of reactions on acyl-CoA thioesters. The thioester O atom is bound in a conserved oxyanion hole. Here, the mode of binding of acyl-CoA substrate analogues to peroxisomal *Saccharomyces cerevisiae* ECI (ScECI2) is described. The best defined part of the bound acyl-CoA molecules is the 3′,5′-diphosphate-adenosine moiety, which interacts with residues of loop 1 and loop 2, whereas the pantetheine part is the least well defined. The catalytic base, Glu158, is hydrogen-bonded to the Asn101 side chain and is further hydrogen-bonded to the side chain of Arg100 in the apo structure. Arg100 is completely buried in the apo structure and a conformational change of the Arg100 side chain appears to be important for substrate binding and catalysis. The oxyanion hole is formed by the NH groups of Ala70 (loop 2) and Leu126 (helix 3). The O atoms of the corresponding peptide units, Gly69 O and Gly125 O, are both part of extensive hydrogen-bond networks. These hydrogen-bond networks are a conserved feature of the crotonase oxyanion hole and their importance for catalysis is discussed.

1. Introduction

The Δ^3,Δ^2-enoyl-CoA isomerases (ECIs) catalyze a critical step in fatty-acid metabolism, facilitating the β-oxidation of unsaturated fatty acids (Hiltunen & Qin, 2000; Zhang *et al.*, 2002; van Weeghel *et al.*, 2012). ECIs catalyze the conversion of 3*E*- and 3*Z*-enoyl-CoA thioesters to 2*E*-enoyl-CoA thioesters (Fig. 1), which are an intermediate in the four-step β-oxidation pathway. Several ECI isoenzymes have been identified (Fig. 1; Geisbrecht *et al.*, 1998, 1999; van Weeghel *et al.*, 2014; Gurvitz *et al.*, 1998; Janssen *et al.*, 1994; Kilponen *et al.*, 1992; Palosaari & Hiltunen, 1990). Mammalian cells contain two mitochondrial enoyl-CoA isomerases (ECI1 and ECI2). ECI2 is also present in peroxisomes. In mammalian peroxisomes a second enoyl-CoA isomerase enzyme is present, the multifunctional enzyme type 1 (MFE1), which also catalyzes two activities of the β-oxidation pathway: the hydratase step (step 2) and the L-3-hydroxyacyl-CoA dehydrogenase step (step 3) (Kasaragod *et al.*, 2010, 2013). The hydratase and the isomerase activities are catalyzed by the N-terminal domain of MFE1 (which adopts the same

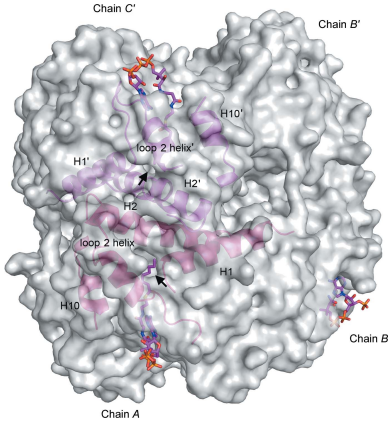

crotonase fold as the monofunctional enoyl-CoA isomerases) and the dehydrogenase step is catalyzed by the C-terminal L-3-hydroxyacyl-CoA dehydrogenase (HAD) part of MFE1 (Zhang *et al.*, 2002; van Weeghel *et al.*, 2012). In the yeast *Saccharomyces cerevisiae* only one enoyl-CoA isomerase is present (Geisbrecht *et al.*, 1998; Hiltunen *et al.*, 2003), which is a peroxisomal isomerase with a peroxisomal targeting signal at its C-terminus (Fig. 1). Sequence comparisons have shown that this isomerase is most closely related to the human ECI2 (Onwukwe *et al.*, 2015) and therefore it will be referred to here as ScECI2. Detailed enzymological characterizations of the rat liver enoyl-CoA isomerases (ECI1, ECI2 and MFE1; Zhang *et al.*, 2002) show that the mammalian ECI2 is a more efficient biocatalyst for long-chain substrates. In recent ECI1-knockout studies in mice it was found that ECI2 can compensate for the loss of ECI1 activity in ECI1-deficient mouse fibroblasts (van Weeghel *et al.*, 2012). This agrees with the notion that both ECI1 and ECI2 are mitochondrial enzymes and that both have relatively broad substrate specificity. The chain-length specificity of ScECI2 has not been so well characterized, but it has been shown that ScECI2 can use 3*Z*-octenoyl-CoA as a substrate (Geisbrecht *et al.*, 1998) as well as 3*E*-hexenoyl-CoA (Gurvitz *et al.*, 1998). In the latter experiments the observed k_{cat} and K_m values were found to be 5.6 s^{-1} and 21.5 μM, respectively. The ScECI2-knockout yeast strain can no longer grow on media with unsaturated fatty acids as a carbon source, but these strains show normal growth in media containing saturated fatty acids. This confirms the critical importance of ScECI2 for the metabolism of unsatutared fatty acids (Hiltunen *et al.*, 2003), and also suggests a broad chain-length specificity. Interestingly, when MFE1 is expressed in these ScECI2-knockout yeast strains, normal growth is seen with polyunsaturated fatty acids as a carbon source (Gurvitz *et al.*, 1998).

The monofunctional ECIs, as well as the hydratase part of MFE1, belong to the hydratase/isomerase (crotonase) superfamily. The members of this superfamily are known to catalyze a wide range of reactions on acyl-CoA thioester substrate molecules (Holden *et al.*, 2001; Hamed *et al.*, 2008). The core of this fold is formed by four repeats of a $\beta\beta\alpha$ unit. The active site is at the N-terminus of helix 3. The crotonase units are assembled as trimers or hexamers (dimers of trimers), but

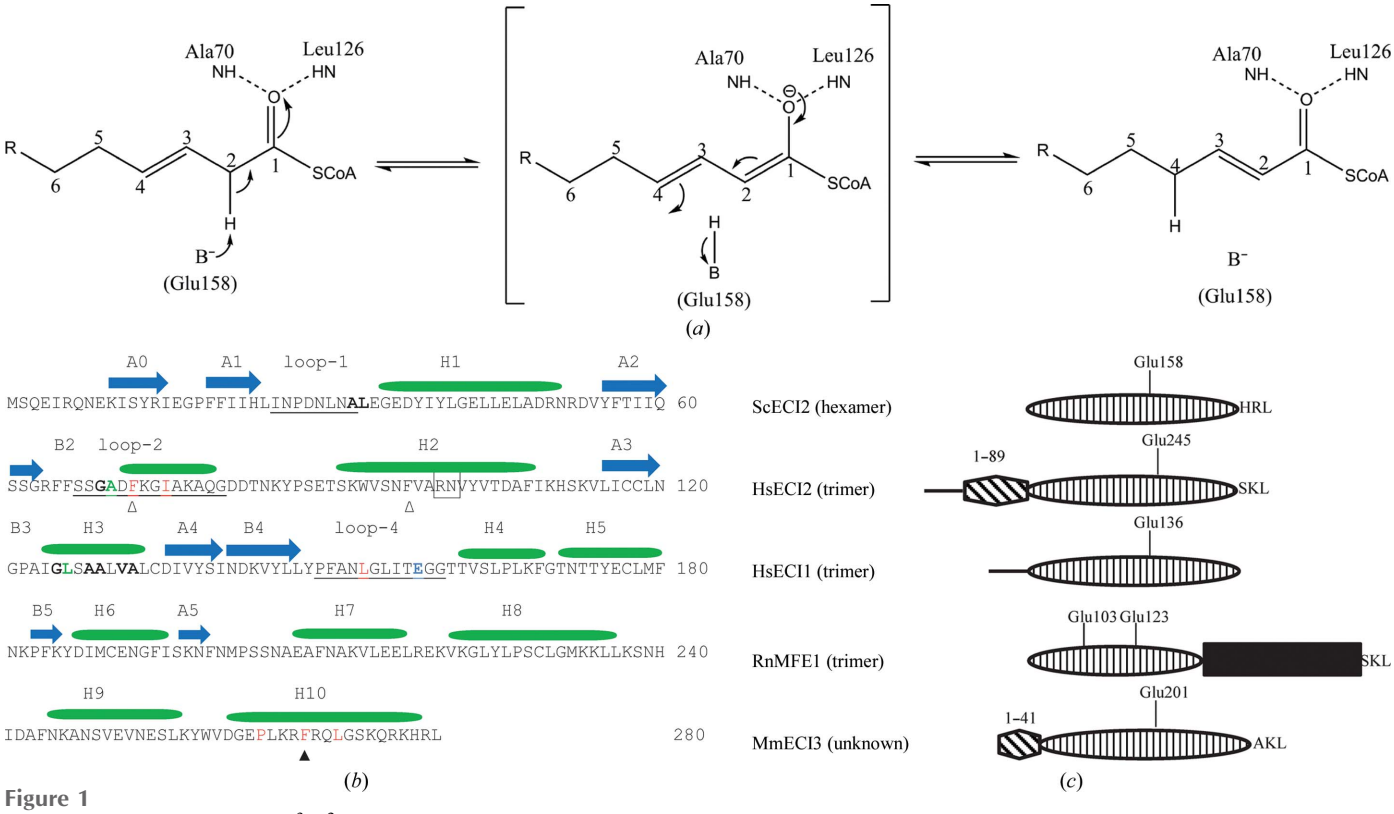

Figure 1
(*a*) The reaction catalyzed by Δ^3,Δ^2-enoyl-CoA isomerase. The catalytic base in ScECI2 is Glu158 and the hydrogen-bond donors of the oxyanion hole are the peptide NH moieties of Ala70 and Leu126. (*b*) The sequence of yeast ECI2. In the construct used in these studies (ScECI2-wt) there are additional tag residues at the N-terminus, as mentioned in §2. The secondary-structure elements are visualized as arrows in blue for the β-strands and as elongated ovals in green for the α-helices. The helical part of loop 2 is referred to in the text as the loop 2 helix. Residues in green provide the oxyanion hydrogen-bond donor peptide NH groups (Ala70 and Leu126). Ala70 also belongs to the hydrophobic cluster; the other residues of the hydrophobic cluster are in red. The catalytic residue (Glu158) is in blue. The important Arg100 and Asn101 residues are in a box. Phe268 of helix 10 is highlighted by a solid triangle. Phe72 and Phe97, discussed in the text, are highlighted by an open triangle. The residues involved in the hydrogen-bond networks of the hydrogen-bond donors of the oxyanion hole are shown in bold (see also Fig. 8). (*c*) The crotonase fold (vertical lines) also occurs as a domain in multi-domain proteins, being extended either at the N-terminus or at the C-terminus by other domains. HsECI2 has an N-terminal ACBP domain (slanted lines) and MFE1 has a C-terminal HAD domain (black). The line at the N-terminus represents the mitochondrial targeting sequence. The labelled C-terminal tripeptides refer to the peroxisomal targeting sequences.

monomers also occur, as in MFE1 (Fig. 1*c*). The active site is covered by the C-terminal helix, also known as helix 10. In each of these enzymes the oxyanion-hole geometry (Hamed *et al.*, 2011, 2012) of the active site is conserved. An important property of such active-site oxyanion holes is that they can stabilize the negative charge formed on the thioester O atom in the transition state of the reaction (Holden *et al.*, 2001; Hamed *et al.*, 2008; Mursula *et al.*, 2001; Fig. 1). The quantitative importance of the oxyanion hole for the stabilization of the transition state has been the subject of many studies (Kamerlin *et al.*, 2010; Pápai *et al.*, 2011; Natarajan *et al.*, 2014). In the ECIs, the negatively charged enolate intermediate is formed following the abstraction of a proton from C2 by a catalytic glutamate acting as a base (Mursula *et al.*, 2001; Partanen *et al.*, 2004; Fig. 1). Enzyme-engineering studies have been undertaken to change the reaction and substrate specificity of crotonase-fold enzymes, such as 4-chlorobenzoyl-CoA dehalogenase (Xiang *et al.*, 1999) and the bacterial carboxymethylproline synthase (CarB; Hamed *et al.*, 2008, 2010, 2011, 2012, 2013).

Recently, we reported the results of structural and enzymological studies of the trimeric human ECI2 (HsECI2; Onwukwe *et al.*, 2015). HsECI2 contains both an N-terminal mitochondrial leader sequence and an additional C-terminal peroxisomal targeting sequence. HsECI2 also has an extra acyl carrier binding protein (ACBP) domain at its N-terminus (Fig. 1), the function of which is not precisely known. The importance of helix 10 for the catalytic properties of HsECI2 appears to be related to the importance of a hydrophobic cluster to which residues of loop 2 and loop 4 contribute, as well as a residue of helix 10 (Phe268 in ScECI2 and Val349 in HsECI2; Onwukwe *et al.*, 2015). A point-mutation variant of this residue (V349A in HsECI2) has much lower catalytic efficiency. Here, we report the structural enzymological properties of ScECI2, which is known to be a hexamer (a dimer of trimers; Mursula *et al.*, 2001). Kinetic data for wild-type and mutated ScECI2 are included, as well as structural data for apo and acyl-CoA-complexed wild-type ScECI2. The mutational studies address the functional importance of the hydrogen-bond networks in the active site and the importance of helix 10 for catalysis. The sequence identity between HsECI2 and ScECI2 is low (22%; Onwukwe *et al.*, 2015). Comparison of the ScECI2 and HsECI2 structures shows that the oxyanion-hole properties are conserved, whereas the detailed interactions of the catalytic base and the mode of binding of the acyl tail are different. Comparisons of the ScECI2 structure with other crotonase-fold enzymes also reveal important conserved features of the hydrogen-bond networks at the oxyanion-hole NH groups at the catalytic site of this fold.

2. Experimental procedures

2.1. Molecular cloning and site-directed mutagenesis

Previously, ScECI2 has been purified and crystallized without a tag using multiple purification steps (Gurvitz *et al.*, 1998; Mursula *et al.*, 2000, 2001) and with a low final yield of purified ScECI2. In order to reduce the number of purification steps and to increase the amount of pure protein, a histidine-tagged construct of ScECI2 was created using restriction-digestion methods. A DNA insert encoding ScECI2 was digested from pET-3a vector using BamHI and NdeI and was ligated into pET-15b vector (Novagen). In the resulting pET-15b-ScECI2 plasmid the mature sequence of ScECI2 (Fig. 1) is preceded by MGSSHHHHHHSSGLVPRGSH, and this construct will be referred to as ScECI2-wt. This plasmid was used as a template for the site-directed mutagenesis experiments. The QuikChange site-directed mutagenesis kit (Agilent Technologies) was used for mutation experiments using PCR technology. From these mutagenesis experiments, the R100A, N101A, N101S and F268A point-mutation ScECI2 variants were generated. A helix 10 deletion variant of ScECI2 (ScECI2-ΔH10) was also created by site-directed mutagenesis by deleting residues 269–280. The primers used for these mutations were the following (mutations are shown in bold): ScECI2-R100A, 5′-GTGGGTGTCGAATTTTGTTGCT**GCA**AATGTTTATGTCACTGATGCC-3′ (forward) and 5′-GGCATCAGTGACATAAACATT**TGC**AGCAACAAAATTCGACACCCAC-3′ (reverse); ScECI2-N101A, 5′-GTGGGTGTCGAATTTTGTTGCTAGA**GCT**GTTTATGTCACTGATGCC-3′ (forward) and 5′-GGCATCAGTGACATAAAC**AGC**TCTAGCAACAAAATTCGACACCCAC-3′ (reverse); ScECI2-N101S, 5′-AGTGGGTGTCGAATTTTGTTGCTAGA**AGT**GTTTATGTCACTGAT-3′ (forward) and 5′-ATCAGTGACATAAAC**ACT**TCTAGCAACAAAATTCGACACCCACT-3 (reverse); ScECI2-F268A, 5′-TGGAGAGCCCTTAAAAAGA**GCA**AGGCAGCTGGGCTCG-3′ (forward) and 5′-CGAGCCCAGCTGCCT**TGC**TCTTTTTAAGGGCTCTCCA-3′ (reverse); ScECI2-ΔH10, 5′-GGGTAGATGGAGAGCCCTTAAAAAGATTT**TGA**CGTCCGCTTTCTCAGTGGAGACCGGCTGC-3′ (forward) and 5′-GCAGCCGGTCTCCACTGAGAAAGCGGACGTCAAA**TCT**TTTTAAGGGCTCTCCATCTACCC-3′ (reverse).

2.2. Enzyme expression and purification

Isolated and purified plasmids were transformed into the *Escherichia coli* BL21*(DE3)pLysS strain and grown at 37°C on plates containing 100 µg ml^{-1} ampicillin and 34 µg ml^{-1} chloramphenicol. A single colony was then used to inoculate 10 ml LB containing antibiotics and the culture was grown at 37°C overnight. The next morning, 5 ml of this culture was used to inoculate 1 l M9ZB medium containing 100 µg ml^{-1} ampicillin and 34 µg ml^{-1} chloramphenicol. Growth was continued until an OD of 0.5 was reached, after which induction was started by adding IPTG to a final concentration of 0.5 m*M*. Induction was performed overnight at 25°C. The next morning, the cells were harvested by centrifugation, resuspended in 50 m*M* HEPES pH 7.5, 300 m*M* NaCl, 1 m*M* *β*-mercaptoethanol, 10% glycerol lysis buffer and kept at −70°C until further use.

ScECI2-wt and its mutated variants were purified using the same protocol.The cells were initially lysed with lysozyme at

Table 1
Crystallization and cryoprotection buffers.

Crystal form	Protein buffer	Well solution	Cryobuffer
ScECI2-CAA (2.6 mg ml^{-1})	30 m*M* HEPES pH 7.5, 100 m*M* NaCl, 5 m*M* acetoacetyl-CoA	100 m*M* MES pH 6.5, 1.6 *M* $(NH_4)_2SO_4$, 10% dioxane	100 m*M* MES pH 6.5, 1.6 *M* $(NH_4)_2SO_4$, 10% dioxane, 20% glycerol, 5 m*M* acetoacetyl-CoA
ScECI2-CO8† (2.6 mg ml^{-1})	30 m*M* HEPES pH 7.5, 100 m*M* NaCl, 1.8 m*M* octanoyl-CoA	100 m*M* HEPES pH 7.0, 1.5 *M* $(NH_4)_2SO_4$	100 m*M* HEPES pH 7.0, 1.5 *M* $(NH_4)_2SO_4$, 20% glycerol, 2.0 m*M* octanoyl-CoA
ScECI2-SO4‡ (2.8 mg ml^{-1})	30 m*M* HEPES pH 7.5, 100 m*M* NaCl, 2 m*M* octanoyl-CoA	100 m*M* sodium citrate pH 5.6, 1 *M* Li_2SO_4, 500 m*M* $(NH_4)_2SO_4$	100 m*M* sodium citrate pH 5.6, 1 *M* Li_2SO_4, 500 m*M* $(NH_4)_2SO_4$, 25% PEG 400, 2 m*M* octanoyl-CoA
ScECI2-F268A (2.7 mg ml^{-1})	30 m*M* HEPES pH 7.5, 100 m*M* NaCl	100 m*M* MES pH 6.5, 1.6 *M* $(NH_4)_2SO_4$, 10% dioxane	100 m*M* MES pH 6.5, 1.6 *M* $(NH_4)_2SO_4$, 10% dioxane, 20% glycerol
ScECI2-ΔH10 (3 mg ml^{-1})	30 m*M* HEPES pH 7.5, 100 m*M* NaCl, 0.2 m*M* decanoyl-CoA	100 m*M* imidazole pH 6.5, 1 *M* sodium acetate	100 m*M* imidazole pH 6.5, 1 *M* sodium acetate, 20% glycerol, 0.2 m*M* decanoyl-CoA

† A white suspension was formed when adding 2 m*M* octanoyl-CoA to the protein sample. ‡ As mentioned in §2, glycerol was used in the purification buffers, except for the protein sample used to obtain the ScECI2-SO4 crystal form.

room temperature (40 min) in the presence of 200 µg ml^{-1} lysozyme, 20 µg ml^{-1} DNase, 2 µg ml^{-1} RNase, 1 m*M* $MgSO_4$ and two tablets of complete protease inhibitor (Roche). The lysates were centrifuged at 35 000*g* for 45 min and the soluble fraction was passed over a Talon column (pre-equilibrated with lysis buffer) at a flow rate of 3 ml min^{-1}. Washing of the column was carried out with 30 m*M* HEPES pH 7.5, 150 m*M* NaCl, 1 m*M* *β*-mercaptoethanol, 10% glycerol, 30 m*M* imidazole with a subsequent gradient elution step using 30 m*M* HEPES pH 7.5, 150 m*M* NaCl, 1 m*M* *β*-mercaptoethanol, 10% glycerol, 500 m*M* imidazole. Fractions containing the recombinant protein were pooled, concentrated and passed through a HiLoad 16/60 Superdex 200 prep-grade size-exclusion chromatographic column (GE Life Sciences) using 30 m*M* HEPES pH 7.5, 100 m*M* NaCl. One additional purification of ScECI2-wt was also performed without any glycerol in the lysis and purification buffers.

2.3. Circular-dichroism measurements

Circular-dichroism (CD) measurements were carried out with ScECI2-wt and its variants using the same protocols as described previously for HsECI2 (Onwukwe *et al.*, 2015). In brief, 30 µg ml^{-1} protein in 10 m*M* potassium phosphate buffer pH 7.5 was used for this experiment in a 400 µl assay volume. The measurements were carried out in the wavelength range from 190 to 260 nm at 20°C using a path length of 0.1 cm. Temperature-dependent denaturation was carried out from 20 to 90°C at a rate of temperature increase of 1°C min^{-1}, performing measurements at steps of 5°C. The instrument used was an Applied Photophysics Chiran Scan. The T_m values were calculated using *Global*3 (Applied Photophysics) using the data at 200–240 nm.

2.4. Enzyme-activity measurements

The Michaelis–Menten parameters for ScECI2-wt were determined as described for HsECI2 by monitoring the formation of NADH at 340 nm in a coupled assay (Onwukwe *et al.*, 2015). The reaction mixture in 50 m*M* Tris–HCl pH 8.5 was composed of 1 m*M* NAD^+, 1.6 µg *Drosophila melanogaster* multifunctional enzyme type 2 (DmMFE2; Haataja *et al.*, 2011), 250 ng ScECI2-wt and 5–200 µ*M* substrate concentration in a total assay volume of 500 µl and the reaction was monitored for 3 min. The measurements were carried out with a Jasco V-660 spectrophotometer. An extinction coefficient of 6220 M^{-1} cm^{-1} was used for the conversion calculations. All experiments were performed at 25°C and at least in triplicate from at least two protein batches, using similar protein concentrations. The data were fitted to the Michaelis–Menten equation using the *GraphFit Prism* software (GraphPad Software).

Specific activity measurements for ScECI2-wt and its mutated variants were carried out at 100 µ*M* 3*E*-decenoyl-CoA substrate concentration. 250 ng ScECI2-wt was used for these measurements, while the amount of the mutated variants used in the assay varied from 1.4 to 4.1 µg. The measurements were performed in duplicate using the same conditions as for the standard assay.

The substrates were prepared as described previously (Onwukwe *et al.*, 2015). Briefly, acyl-CoA thioesters were prepared by the mixed-anhydride method (Rasmussen *et al.*, 1990) and purified on reverse-phase silica gel (RP-18; ICN Chemicals, Costa Mesa, California, USA). The substrate purity was verified by high-resolution electrospray ionization Fourier transform ion cyclotron (ESI-FTICR) mass spectrometry (APEX II, Bruker, Bremen).

2.5. Crystallization, data collection and structure refinement

Crystallization experiments were performed at room temperature using a protein sample buffer consisting of 30 m*M* HEPES pH 7.5, 100 m*M* NaCl. The ScECI2-wt samples were co-crystallized in the presence of 5 m*M* acetoacetyl-CoA or 1.8 m*M* octanoyl-CoA, whereas the ScECI2-ΔH10 sample was co-crystallized in the presence of 0.2 m*M* decanoyl-CoA (Table 1). Another ScECI2-wt sample, purified without glycerol in the purification buffers, was also used in crystallization experiments aimed at obtaining a glycerol-free ScECI2 structure. Crystallization trials were set up by mixing 0.5 µl of the enzyme–ligand complex with 0.5 µl well solution by the sitting-drop vapour-diffusion method using 50 µl well solution. The crystallization setups were prepared using a

Table 2
The data-collection and refinement statistics for the five ScECI2 crystal structures.

Values in parentheses are for the highest resolution shell.

	ScECI2-CAA	ScECI2-CO8	ScECI2-SO4	ScECI2-F268A	ScECI2-ΔH10
Data-collection statistics					
Processing software	*XDS*, *AIMLESS*	*XDS*, *AIMLESS*	*XDS*, *AIMLESS*	*XDS*, *AIMLESS*	*XDS*, *AIMLESS*
Beamline	P13, DESY	ID29, ESRF	I04-1, DLS	P13, DESY	ID29, ESRF
Wavelength (Å)	0.945	0.976	0.920	0.945	0.976
Space group	$P4_12_12$	$P4_12_12$	$P6_322$	$P4_12_12$	$P321$
Unit-cell parameters (Å)	$a = b = 116.9$, $c = 218.6$	$a = b = 117.3$, $c = 219.4$	$a = b = 116.0$, $c = 122.0$	$a = b = 116.7$, $c = 219.7$	$a = b = 118.1$, $c = 87.4$
No. of subunits per asymmetric unit	3	3	1	3	2
Resolution range (Å)	103.10–2.14 (2.18–2.14)	47.31–2.13 (2.17–2.13)	77.60–3.00 (3.18–3.00)	116.70–2.10 (2.14–2.10)	48.94–1.81 (1.87–1.81)
Completeness (%)	99.5 (91.1)	99.8 (97.4)	100.0 (100.0)	100.0 (100.0)	99.7 (97.2)
$\langle I/\sigma(I)\rangle$	14.0 (2.0)	12.6 (1.7)	8.9 (2.2)	10.7 (1.3)	17.3 (1.6)
$R_{\rm p.i.m.}$ (%)	3.3 (33.2)	3.8 (47.0)	4.8 (28.5)	5.5 (63.1)	2.3 (43.3)
No. of unique reflections	83764 (4136)	86227 (4412)	10249 (1609)	89154 (4502)	64106 (6063)
Multiplicity	14.3 (6.1)	7.3 (7.2)	21.2 (22.8)	14.9 (15.1)	10.5 (6.7)
Matthews coefficient (Å^3 Da^{-1})	3.7	3.7	3.5	3.9	2.7
Wilson *B* factor (Å^2)	30.7	37.2	83.7	32.0	30.3
Refinement statistics					
Resolution (Å)	103.10–2.14	47.31–2.13	40.00–3.00	80.12–2.10	48.94–1.81
$R_{\rm work}$ (%)	16.49	16.81	17.24	17.47	15.92
$R_{\rm free}$ (%)	19.01	19.02	22.30	19.70	18.79
No. of reflections ($R_{\rm work}$)	79476	81724	9688	84599	60689
No. of reflections ($R_{\rm free}$)	4184	4307	532	4455	3239
No. of atoms	7001	6946	1992	6710	4478
No. of waters	416	353	9	433	305
No. of ligand molecules					
CAA	3	—	—	—	—
CO8	—	3	—	—	—
SO4	8	10	3	14	—
GOL	7	8	—	3	1
Geometry statistics					
R.m.s.d., bonds (Å)	0.014	0.013	0.013	0.013	0.013
R.m.s.d., angles (°)	1.7	1.6	1.6	1.6	1.4
Average *B* factor (Å^2)					
Protein atoms	39.8	47.1	63.1	41.4	35.5
Waters	44.1	49.3	49.5	46.8	43.0
CAA	88.7	—	—	—	—
CO8	—	100.0	—	—	—
SO4	71.0	84.4	117.5	73.1	—
GOL	54.0	62.4	—	57.5	61.4
Ramachandran plot† (%)					
Favoured	96.4	96.2	94.7	97.0	96.6
Allowed	3.3	3.7	5.3	2.7	2.8
Outliers	0.3	0.1	0.0	0.3	0.6
PDB entry	4zdb	4zdc	4zdd	4zde	4zdf

† The Ramachandran values are as calculated by *MolProbity* (Chen *et al.*, 2010).

Mosquito crystallization robot (TTP Labtech) and the plates were stored and imaged in a Formulatrix RI54 plate hotel. The crystallization results were monitored using the *xtalPiMS* software (Daniel, Morris, Wierenga *et al.*, manuscript in preparation). Crystals were cooled in-house in liquid nitrogen and shipped to synchrotrons for data collection. Before cooling, the crystals were briefly passed through a cryobuffer [well solution supplemented with the co-crystallization ligand and with 20% glycerol or polyethylene glycol (PEG) 400] (Table 1). A total of five crystal structures were obtained (Table 2): three ScECI2-wt crystals, an octanoyl-CoA complex and an acetoacetyl-CoA complex. The octanoyl-CoA and acetoacetyl-CoA structures are referred to as ScECI2-CO8 and ScECI2-CAA, respectively. In the third ScECI2-wt crystal form, which was purified and cryoprotected in the absence of glycerol, a sulfate (SO_4^{2-}) ion was present in the active site. This structure is referred to as the ScECI2-SO4 structure. Only apo structures were obtained in the crystallization experiments using the helix 10 variants (ScECI2-F268A and ScECI2-ΔH10). The data collections were carried out at several synchrotron beamlines (Table 2). The data processing and scaling of the complexed structures of ScECI2-wt and the apo structures of the helix 10 variants were carried out using *XDS* (Kabsch, 2010) and *AIMLESS* (Evans & Murshudov, 2013) from the *CCP*4 protein crystallography software suite (Winn *et al.*, 2011). The ScECI2-SO4 data were processed using the automatic processing software package *xia*2 (Winter, 2010) at the Diamond Light Source (DLS). All structures were refined with *REFMAC*5 (Murshudov *et al.*, 2011). For all structures NCS restraints were imposed, except for the ScECI2-SO4

Table 3
The Michaelis–Menten parameters for ScECI2-wt.

The standard deviations are based on at least three independent experiments.

Substrate	K_m (μM)	k_{cat} (s^{-1})	k_{cat}/K_m ($s^{-1}\ M^{-1}$)
3*E*-Hexenoyl-CoA	72.0 ± 11.0	1.7 ± 0.2	0.2×10^5
3*E*-Decenoyl-CoA	50.0 ± 5.1	4.4 ± 0.3	0.9×10^5

structure, in which there is only one subunit per asymmetric unit. In all cases model building was performed with *Coot* (Emsley & Cowtan, 2004). The data-processing and refinement statistics are listed in Table 2.

2.6. Structure analysis

The crystal structures were analyzed with *Coot* (Emsley & Cowtan, 2004) and *MolProbity* (Chen *et al.*, 2010). Structural comparisons were performed with two apo structures of ScECI2: PDB entries 1pjh (chain *A*, 2.1 Å resolution; Mursula *et al.*, 2004) and 1hno (2.5 Å resolution; Mursula *et al.*, 2001). In the 1pjh structure a glycerol is bound in the active site and this structure will be referred to as the 1pjh apo structure. In this crystal form the trimers are tightly packed into a hexamer, as also observed in solution (Mursula *et al.*, 2001). In the 1hno structure the trimers are loosely packed into a hexamer, which is believed to be a crystallographic artefact (Mursula *et al.*, 2001). In the active site of the latter structure a water molecule is bound in the oxyanion hole and this structure will be referred to as the 1hno apo structure. The structure 1pjh is from crystals obtained at pH 7.0 in the presence of 0.1 *M* $MgSO_4$ and 1.7 *M* ammonium sulfate and cryoprotected by adding 20% glycerol. The 1hno crystals were grown at pH 5.6 in the presence of 5% 1,4-dioxane and 1.4 *M* ammonium sulfate; 20% ethylene glycol was added for cryoprotection.

The other members of this superfamily that were used for comparison are rat MFE1 (PDB entry 3zwc, chain *A*, complexed with 3-hydroxydecanoyl-CoA, 2.3 Å resolution; Kasaragod *et al.*, 2013), rat enoyl-CoA hydratase (PDB entry 2dub, chain *A*, complexed with octanoyl-CoA, 2.4 Å resolution; Engel *et al.*, 1998), human ECI1 (PDB entry 1sg4, chain *B*, complexed with octanoyl-CoA, 1.3 Å resolution; Partanen *et al.*, 2004), human HsECI2 (PDB entry 4u18, chain *A*, apo, 2.6 Å resolution; Onwukwe *et al.*, 2015), CarB (PDB entry 2a81, chain *A*, 3.2 Å resolution; Sleeman *et al.*, 2005) and bacterial 4-chlorobenzoyl-CoA dehalogenase (PDB entry 1nzy, chain *A*, 1.8 Å resolution; Benning *et al.*, 1996). For the ScECI2 structures subunit *A* has been used for the comparison studies in each case.

3. Results and discussions

3.1. Stability and catalytic properties of ScECI2

Wild-type ScECI2 and its mutated variants were purified to homogeneity using an immobilized metal-affinity chromatography (IMAC) step followed by gel filtration. The CD melting curves of the purified ScECI2 variants, measured as described in §2, show a T_m value of 67.0°C for ScECI2-wt, whereas the T_m values of the other variants range from 63.8 to 53.3°C (Fig. 2). The N101S and N101A variants have the lowest T_m values of 54.3 and 53.3°C, respectively. In these experiments the unfolding is irreversible and therefore it is not possible to infer conclusions concerning the relative thermodynamic stability of these variants. The k_{cat} and K_m values of ScECI2 were determined for the substrates 3*E*-hexenoyl-CoA and 3*E*-decenoyl-CoA (Table 3). For 3*E*-hexenoyl-CoA the k_{cat} and K_m values are 1.7 s^{-1} and 72 μM, respectively. It is noted that the k_{cat} values for ScECI2 are about fivefold lower than for HsECI2 (Onwukwe *et al.*, 2015), whereas the corresponding K_m values are very similar. The k_{cat} of ScECI2 for 3*E*-decenoyl-CoA is about three times higher than for the shorter 3*E*-hexenoyl-CoA substrate (Table 3) and the k_{cat}/K_m ratio is also about three times higher for the longer chain substrate. Additional activity measurements in the presence of 100 μM 3*E*-hexenoyl-CoA and 100 μM 3*E*-decenoyl-CoA, respectively, show that both helix 10 and the active-site point mutation variants have much lower activity than ScECI2-wt (Table 4), as discussed further in subsequent sections. The

Table 4
The specific activity of ScECI2-wt and its variants at 100 μM 3*E*-decenoyl-CoA concentration.

ND, not detectable.

Enzyme	Substrate	Specific activity (μmol min^{-1} mg^{-1})
ScECI2-wt	3*E*-Hexenoyl-CoA	1.93 ± 0.02
	3*E*-Decenoyl-CoA	4.40 ± 0.09
ScECI2-F268A	3*E*-Hexenoyl-CoA	0.26 ± 0.01
	3*E*-Decenoyl-CoA	0.35 ± 0.02
ScECI2-ΔH10	3*E*-Hexenoyl-CoA	ND
	3*E*-Decenoyl-CoA	ND
ScECI2-N101A	3*E*-Hexenoyl-CoA	0.50 ± 0.05
	3*E*-Decenoyl-CoA	0.62 ± 0.04
ScECI2-N101S	3*E*-Hexenoyl-CoA	ND
	3*E*-Decenoyl-CoA	ND
ScECI2-R100A	3*E*-Hexenoyl-CoA	0.93 ± 0.05
	3*E*-Decenoyl-CoA	0.40 ± 0.04

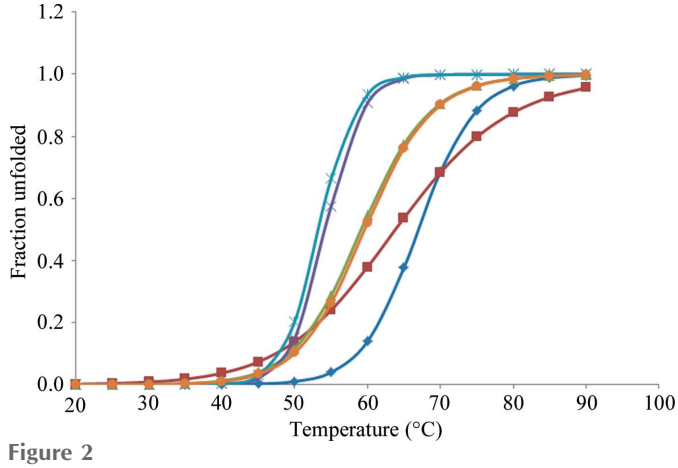

Figure 2
The CD melting curves of ScECI2-wt (dark blue, T_m = 67.0°C) and its various mutated variants: F268A (red, T_m = 63.8°C), R100A (orange, T_m = 59.6°C), ΔH10 (green, T_m = 59.2°C), N101A (purple, T_m = 54.3°C) and N101S (light blue, T_m = 53.3°C).

compounds acetoacetyl-CoA and octanoyl-CoA used in the crystallographic binding studies (see the next section) are substrate analogues. Indeed, in enzyme-activity assays, these compounds were found to be inhibitors: at 2 m*M* ligand concentration approximately 20% activity remains.

3.2. Crystallographic binding studies with acetoacetyl-CoA and octanoyl-CoA

The crystal forms of these complexes of ScECI2-wt were obtained by co-crystallization experiments in the presence of 5 m*M* acetoacetyl-CoA and 1.8 m*M* octanoyl-CoA, respectively (Table 1). The structures of these complexes were both refined at 2.1 Å resolution (Table 2). In both structures there is a trimer in the asymmetric unit, and a hexameric assembly is generated by crystallographic symmetry operations, which is the same as described for the 1pjh apo structure (Mursula *et al.*, 2004). *PISA* calculations (Krissinel & Henrick, 2007) with the 1pjh apo structure predict that the hexamer has been crystallized in this crystal form. The crystals were cryocooled in a mother liquor to which 20% glycerol had been added (Table 1), as in the 1pjh apo structure determination. In the latter structure a glycerol is bound in the active site. In the initial electron-density OMIT maps of the ScECI2-CAA and ScECI2-CO8 structures, the 3′,5′-diphosphate-adenosine moiety of CoA was clearly visible (Fig. 3). Apparently, this moiety contributes significantly to the affinity of the substrate. This has also been characterized for another CoA-dependent enzyme, succinyl-CoA:3-ketoacyl-CoA transferase (SCOT; Whitty *et al.*, 1995; Moore & Jencks, 1982). For this enzyme it was shown that the pantetheine moiety is important for activation, although it has only weak binding interactions, whereas the 3′,5′-diphosphate-adenosine moiety is not important for activation but does provide the binding energy for the pantetheine part to bind and activate the substrate (Jencks, 1987), as reviewed recently (Amyes & Richard, 2013). The initial electron-density maps of the catalytic site also showed electron density for a ligand: either for a glycerol or for a fatty-acyl tail or for a mixture. After extensive refinement calculations, testing different hypotheses concerning the possible modes of binding of these ligands, it was found that the electron-density maps of the ScECI2-CAA structure agree best with a close to 100% occupancy of an outward-bound conformation of the acetoacetyl moiety (Fig. 3*a*), whereas in the ScECI2-CO8 structure an

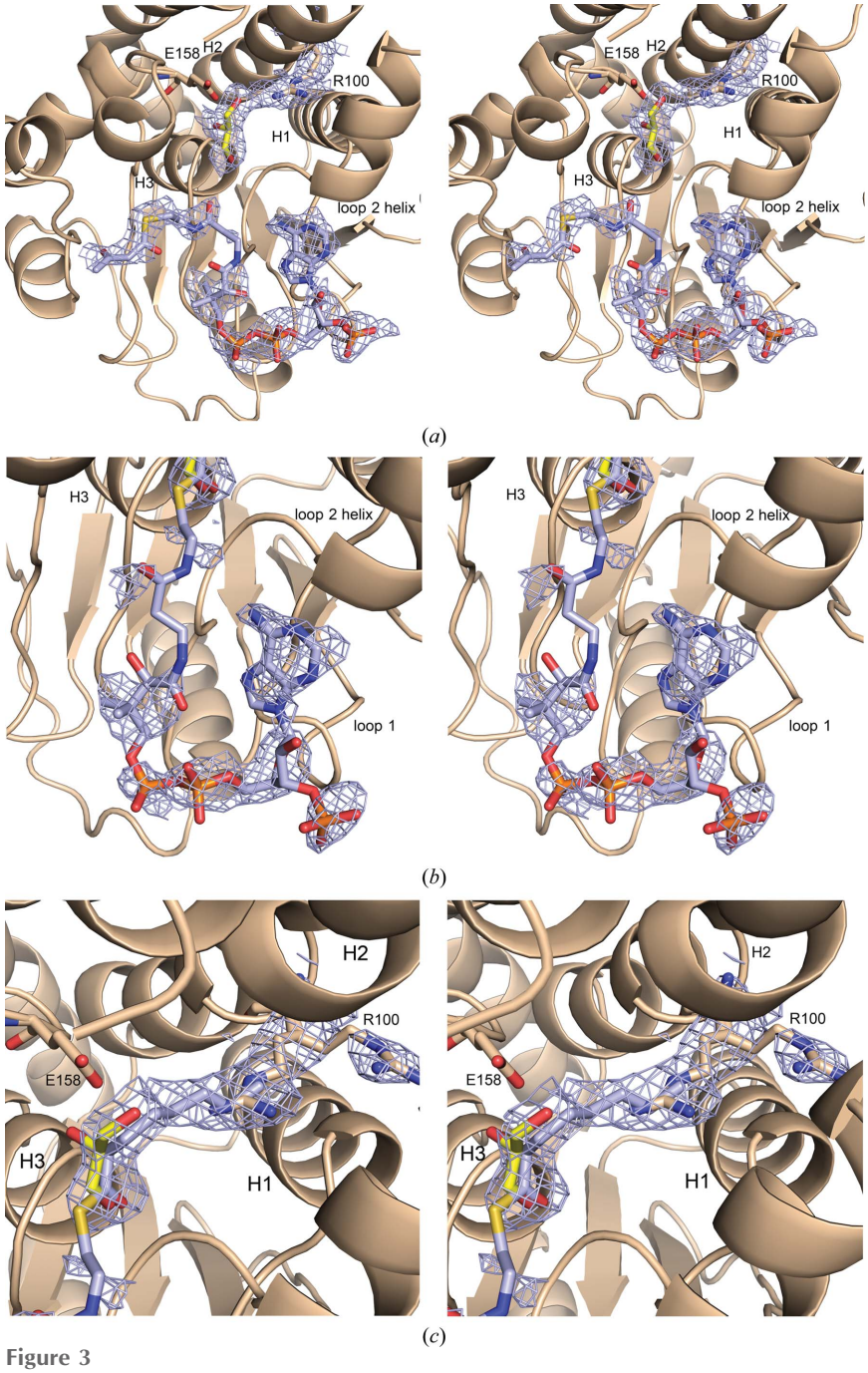

Figure 3
The major modes of binding of the acyl-CoA substrate analogues to ScECI2. The superimposed ($F_o - F_c$) OMIT density maps (calculated after OMIT refinement) are contoured at 2.0σ. (*a*) Stereo image of the ScECI2-CAA crystal structure showing the outward-pointing mode of binding of acetoacetyl-CoA, the active-site glycerol (yellow) and the inward-pointing Arg100. (*b*) Stereo image of the ScECI2-CO8 crystal structure showing the inward-pointing mode of binding of octanoyl-CoA. (*c*) Stereo image of the ScECI2-CO8 crystal structure visualizing the inward mode of binding of the acyl tail and the two conformations of the Arg100 side chain. This mode of binding of the acyl moiety of octanoyl-CoA (the occupancy is 0.6) overlaps with the mode of binding of the active-site glycerol molecule (the occupancy is 0.4; yellow) and with the inward-pointing Arg100 side chain (the occupancy is 0.4). The acyl tail of the octanoyl-CoA adopts a bent conformation, corresponding to a possible mode of binding of the 3*Z*-octenoyl-CoA substrate.

inward-bound conformation is clearly present in subunits *A* and *C* (Figs. 3*b* and 3*c*). The pantetheine moiety could be built in electron density in the $2F_o - F_c$ map, being best defined in subunit *A*. In this inward-pointing conformation the position of the thioester oxygen moiety in the oxyanion hole is well defined. The mode of binding of the acyl chain overlaps with the inward-pointing conformation of the Arg100 side chain of helix 2. The best refinement results are obtained when the occupancies of the inward-bound conformations of the acyl chain and the arginine side chain are set to 0.6 and 0.4, respectively (Fig. 3*c*). The guanidine moiety of the outward-pointing side chain of Arg100 interacts with Glu36 (OE2 atom) and Asn96 (O atom) of the same subunit. When the Arg100 side chain is in its flipped-out position then a tunnel is formed between the catalytic site and the bulk solvent. This tunnel is lined clockwise by the side chains of residues Phe97 (helix 2), Asn101 (helix 2), Arg100 (helix 2), Ala70 (loop 2), Ile75 (loop 2), Phe268 (helix 10) and Trp259 (helix 9) (Fig. 4). This mode of binding of the fatty-acyl tail in a tunnel between the catalytic site and bulk solvent has also been observed for HsECI2 (Onwukwe *et al.*, 2015) and HsECI1 (Partanen *et al.*, 2004). It is consistent with a broad chain-length specificity of ScECI2. The octanoyl tail is bound in a bent conformation (Fig. 3*c*), as the C2—C3—C4—C5 dihedral angle is close to zero, corresponding to the 3*Z* conformation of the actual substrate (3*Z*-enoyl-CoA). Kinetic data for 3*Z* substrates of ScECI2 have only been reported for 3*Z*-octenoyl-CoA (Geisbrecht *et al.*, 1998), with a rate of 8 s^{-1} at 30 μ*M* substrate concentration (Binstock & Schulz, 1981), which is higher than reported in Table 3 for 3*E*-hexenoyl-CoA and 3*E*-decenoyl-CoA substrates. *In vivo*, the occurrence of 3*Z*-enoyl-CoA is much more predominant than 3*E*-enoyl-CoA (Hiltunen *et al.*, 2003). The structural and kinetic data suggest that the 3*Z*-enoyl-CoA is indeed the better substrate.

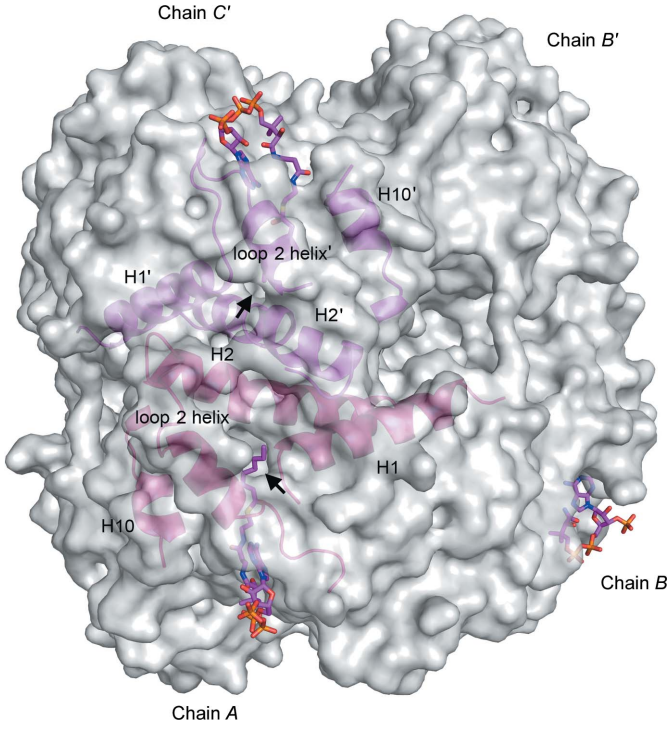

Figure 4
A surface representation of the ScECI2-CO8 hexamer. The hexamer is composed of two trimers. Chains *A*, *B* and *C* form the lower trimeric disc and *A*′, *B*′ and *C*′ form the upper trimeric disc. Octanoyl-CoA molecules in the *A*, *B* and *C*′ subunits are shown as sticks. The exit tunnel (shown by arrows in subunits *A* and *C*′) for the fatty-acyl tail is formed by loop 1, H1, H2 and the loop 2 helix (shown as ribbons in chains *A* and *C*′). Helix 10, covering the pantetheine part of the octanoyl-CoA molecule, is also highlighted. The inward-pointing Arg100 side chain and the glycerol in the active site were omitted in these surface calculations.

There are no conformational differences near the catalytic site when the 1pjh apo structure is compared with the two liganded structures, except for Arg100, which adopts a double conformation in the octanoyl-CoA complexed structure. Comparison of the two liganded structures with the 1pjh apo structure only shows structural differences in loop 2, which is partly disordered in the apo structure and is completely built in the acetoacetyl-CoA and octanoyl-CoA complex structures. In addition, the Phe72 side chain adopts a double conformation in the 1pjh apo structure, whereas in the liganded structures it is only present in the conformation which is stacked against the adenine ring (Fig. 5). The loop 2 region nearest to the catalytic site (residues Asp71–Lys77) adopts a helical conformation (Fig. 1) and this loop 2 helix is well defined in each of the three structures, whereas Ala78–Asn84 were not built in the 1pjh apo structure; these residues are present in the liganded structures as high *B*-factor regions. The well defined part of loop 2, together with loop 1, shapes the binding pocket for the adenine moiety of CoA (Fig. 5, Table 5).

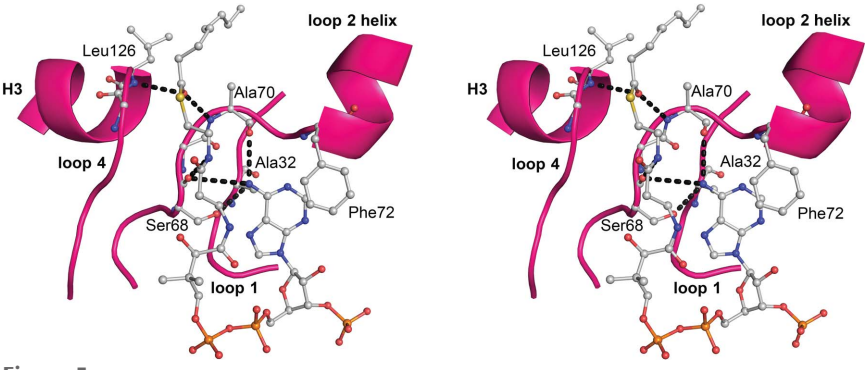

Figure 5
The mode of interaction of the 3′,5′-diphosphate-adenosine, pantetheine and thioester moieties in ScECI2. The 3′,5′-diposphate-adenosine part of the octanoyl-CoA molecule in the ScECI2-CO8 crystal structure is sandwiched between Phe72 of the loop 2 helix structure and Ala32 of loop 1. The hydrogen bonds between the amino group of the adenine and the carbonyl O atoms of Ser68 and Ala70 (both residues from loop 2) are a conserved feature in the crotonase superfamily (Table 5). Ala70 is also important in oxyanion-hole formation for the thioester moiety together with Leu126 (at the N-terminus of H3). Dotted lines visualize hydrogen-bond interactions.

The mode of binding of the tail moiety of octanoyl-CoA is different when compared with the HsECI1 complex (Fig. 6*a*), whereas the CoA moieties bind in the same bent

Table 5
Interactions of the acyl-CoA moiety with loop 1, loop 2, helix 3 and loop 4.

Enzyme	Yeast ECI2	Human ECI1	Rat MFE1	Rat enoyl-CoA hydratase	Bacterial dehalogenase	Bacterial CarB
PDB code (chain identifier)	4zdc (*A*)	1sg4 (*B*)	3zwc (*A*)	2dub (*A*)	1nzy (*A*)	2a81 (*A*)
The two side chains forming the adenine-binding pocket						
Loop 1	Ala32	Ser27	Ala23	Ala60	Ala26	Pro23
Loop 2	Phe72	Leu68	Ile63	Ile100	Leu66	Phe64†
The hydrogen-bond acceptors for the adenine NH_2 group						
Loop 2	Ser68 O	Ala64 O	Ala59 O	Ala96 O	Ala62 O	Ala60 O
Loop 2	Ala70 O	Leu66 O	Ala61 O	Ala98 O	Phe64 O	Gly62 O
Hydrogen-bond acceptor for the pantetheine N4						
Loop 2	Ser68 O	Ala64 O	Ala59 O	Ala96 O	Ala62 O	‡
Hydrophobic cluster near the thioester moiety						
Loop 2	Ala70/Phe72/Ile75	Leu66/Leu68/Met71	Ala61/Ile63/Phe66§	Ala98§/Ile100§/Met103§	Phe64/Leu66/Ile69	‡
Helix 10	Pro264/Phe268	Leu248	Phe271	Met276/Phe279	Phe245/Leu249/Phe252	‡
Loop 4	Pro149/Leu153§	Leu139§/Ile141	Leu126§/Ile128	Leu167§/Thr169	Ile140§/Ile142	‡
Main-chain peptide NH groups forming the oxyanion hole						
Loop 2	Gly69-Ala70 N	Gly65-Leu66 N	Gly60-Ala61 N	Gly97-Ala98 N	Gly63-Phe64 N	Gly61-Gly62 N¶
Helix 3	Gly125-Leu126 N	Ala110-Gly111 N	Gly99-Gly100 N	Gly140-Gly141 N	Gly113-Gly114 N	Gly107-Met108 N¶

† The hydrophobic side chain of Phe64 is near the adenine ring, but it points into bulk solvent. ‡ Only the 3′,5′-diphosphate-adenosine part is well ordered and could be built in the electron-density map. § This hydrophobic side chain contacts the acyl-CoA S atom (within 4.2 Å). ¶ As identified from interactions with the O atom of the bound buffer molecule bicin.

conformations. This mode of binding of the tail is also somewhat different to that observed in corresponding structures of other ligand-bound complexes of crotonase-fold enzymes (Onwukwe *et al.*, 2015). The most conserved feature of these complexes is the binding of the thioester O atom in the oxyanion hole and the mode of binding of the adenine moiety. In particular, the hydrogen-bond interactions of the adenine NH_2 moiety with loop 2 main-chain O atoms (Table 5, Fig. 5) are well conserved, as discussed further in the next sections. In the ScECI2-CO8 complex the pantetheine moiety is least well defined by its electron density, but like in the other structures (Table 5) its peptide N4 atom is hydrogen-bonded to Ser68 O of loop 2 (Fig. 5).

The closest homologue of ScECI2 is HsECI2, although its sequence identity is rather low (Onwukwe *et al.*, 2015). In each of the three isomerases (HsECI1, HsECI2 and ScECI2) the catalytic base is a glutamate. In HsECI1 and HsECI2 this side chain is anchored by a hydrogen bond to one of its carboxylate O atoms (to its own main-chain peptide NH moiety), whereas in the active site of ScECI2-CO8 both carboxylate O atoms of Glu158 are hydrogen-bonded (to a water and Asn101, respectively; Fig. 6*a*). It can also be noted that the orientation of the carboxylate moiety of the catalytic glutamate with respect to the acyl chain, as observed in ScECI2-CO8, is different from the HsECI1–octanoyl-CoA complex (Fig. 6*a*). Small differences of the interactions between the side chains of Glu158 and Asn101 are observed in the 1hno apo complex and in the ScECI2-CO8 complex (Fig. 6*b*), as discussed further in the next sections.

3.3. Crystal structure of a trimeric complex with sulfate bound in the active site

In the crystal structures of ScECI2-CAA and ScECI2-CO8 a glycerol is bound in the active site, competing with proper ligand binding. Therefore, crystallization experiments were also set up in which glycerol was not used as cryoprotectant. Suitable crystals were grown using 1 *M* lithium sulfate, 100 m*M* sodium citrate pH 5.6, 500 m*M* ammonium sulfate and 2 m*M* octanoyl-CoA as a well solution and 10% PEG 400 as cryoprotectant (Table 1). From these crystals a 3.0 Å resolution data set could be collected (Table 2). In these ScECI2-SO4 crystals, which are isomorphous to the previously characterized apo crystals, there is one subunit per asymmetric unit. As in the 1hno apo crystal form (Mursula *et al.*, 2001), on applying the symmetry operations a hexameric assembly is formed consisting of two trimers, which form a loose, crystallographic hexamer. Indeed, *PISA* calculations with the 1hno apo structure predict that in this crystal form it is the trimer that has been crystallized. In this mode of assembly the trimers are further apart than in the tight hexamer (Mursula *et al.*, 2004). This different packing of the two trimers is correlated with a conformational switch of the N-terminal part of helix 2 (residues Ser88–Tyr103): in the 1hno apo form helix 2 is straight, whereas in the 1pjh apo form helix 2 is bent (Fig. 7). Helix 2 is at the inter-trimer interface of the tight hexamer, interacting with the symmetry-related helix 2 of the other trimer (Mursula *et al.*, 2004; Fig. 7). The structural change of helix 2 not only weakens the inter-trimer contacts, but also causes small rearrangements in the side-chain positions of Asn101 and Arg100 (Fig. 6*c*). Further changes are also noted for loop 2 (the region 74–89, including the loop 2 helix, is disordered in the ScECI2-SO4 structure), whereas the C-terminal end of helices 9 and 10 have shifted by about 1.5 Å upwards, away from the active site (Fig. 7). There is only weak electron density for the 3′,5′-diphosphate-adenosine part of CoA, and this moiety was not included in the refined model. A sulfate ion bound in the oxyanion hole is hydrogen-bonded to the inward-pointing Arg100 side chain (Fig. 6*c*). The rearrangement of the N-terminal end of helix 2 also correlates with differences in the side-chain positions of Trp93 (helix 2) and Phe97 (helix 2) as well as Phe72 (loop 2), Ile75 (loop 2, disordered), Trp259 (helix 9) and Phe268 (helix 10). In this ScECI2-SO4 structure, Phe72, which covers the adenine part

in the octanoyl-CoA complex, now points inwards (Fig. 7). Very similar structural changes are also seen in the 1hno apo trimer, but in this structure the Arg100 side chain points outwards. Apparently, in the trimeric (loose hexameric) state, as in the tight hexameric assembly, the Arg100 side chain can adopt an inward-pointing position as well as an outward-pointing position.

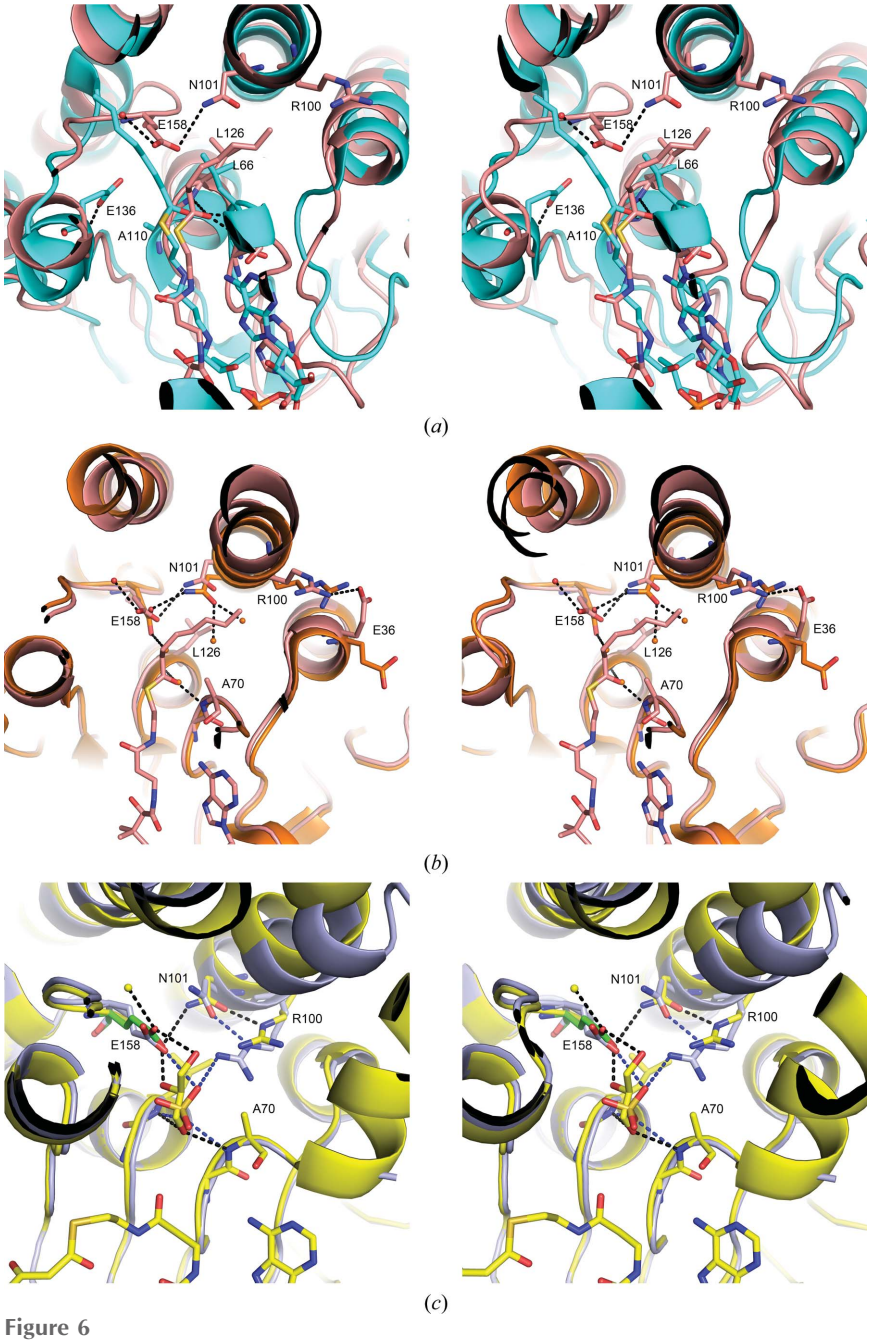

Figure 6
Hydrogen-bond network in the active site of ScECI2 crystal structures. Dotted lines visualize hydrogen-bond interactions. (*a*) The active site of ScECI2 complexed with octanoyl-CoA (reddish; glycerol and the inward-pointing Arg100 side chain are not shown) aligned with the active site of the octanoyl-CoA complex of human ECI1 (cyan; PDB entry 1sg4). The figure highlights the different binding modes of the fatty-acyl tail, as well as the different anchoring hydrogen-bond networks of the catalytic glutamate in these two isomerase structures (Glu136 in HsECI2 and Glu158 in ScECI2). Notably, the catalytic glutamates are in different positions of loop 4, whereas the positions of the oxyanion-hole residues are conserved. (*b*) The mode of interaction of Glu158, Asn101 and Arg100 (in outward-pointing conformation) in the ScECI2-CO8 structure (tight hexamer; reddish) and the loose hexamer form of apo ScECI2 (orange; PDB entry 1hno). (*c*) The mode of interaction of Glu158–Asn101–Arg100 in the active site of the ScECI2-CAA complex (yellow) and the ScECI2-SO4 apo form (light blue). Glycerol in the active site of 1hno apo, sulfate in the active site of ScECI2-SO4 apo and the inward-pointing Arg100 of both structures are also shown.

3.4. Structural enzymology studies of the helix 10 variants

As in HsECI2, the hydrophobic side chain of helix 10 (Phe268) is part of a hydrophobic cluster (Fig. 1*b*, Table 5) that covers the thioester moiety and provides binding interactions with the ligand, in particular with the S atom of its thioester moiety (Table 5). Therefore, the same variants as prepared for HsECI2 were also prepared for ScECI2: a point-mutation variant (F268A) and a deletion variant (deletion of the C-terminal residues Arg269–Leu280). As for HsECI2, the point-mutation variant is slightly active and the helix 10 deletion variant is inactive (Table 4). The crystal structures, refined at 2.1 Å resolution (ScECI2-F268A) and 1.8 Å resolution (ScECI2-ΔH10), show that the trimeric and tight hexameric assemblies are identical to those in the 1pjh apo structure, although the crystal packing is different for the ScECI2-ΔH10 structure. The structural differences involve loop 2 and helix 10. Helix 10 does not change its conformation, but its mutations generate an empty volume that is filled by the Phe72 (loop 2) side chain in both structures, which rotates inwards, adopting the position previously occupied by the Phe268 side chain. This movement of Phe72 is also seen in the ScECI2-SO4 structure (Fig. 7), whereas in the 1pjh apo structure both conformations are observed. An additional change in loop 2 involves Ile75, which moves away from the ligand (in the point-mutation variant) or is disordered (in the deletion variant). These structural changes disrupt the hydrophobic cluster which interacts with the thioester moiety in the liganded ScECI2-wt structures. This disruption of the hydrophobic cluster apparently causes the decreased catalytic efficiencies of these two variants, as in HsECI2 (Onwukwe *et al.*, 2015).

3.5. The hydrogen-bond network at the catalytic site

The structure of ScECI2-CO8 visualizes the positioning of the side chain of the

catalytic base, Glu158, with respect to the acyl moiety of the substrate analogue. In all structures the catalytic base is hydrogen-bonded to the Asn101 side chain (Fig. 6). In the apo structure with glycerol bound in the active site of the ScECI2-CAA complex, Glu158 OE2 is hydrogen-bonded to a water molecule and Glu158 OE1 is hydrogen-bonded to O2 of glycerol and to Asn101 ND1. Asn101 OD2 is subsequently hydrogen-bonded to Arg100 NE. This hydrogen-bond network from Glu158 *via* Asn101 to Arg100 will affect the pK_a of the Glu158 side chain and therefore is relevant to the protonation state of this catalytic glutamate. The positively charged Arg100 side chain will favour deprotonation of Glu158. The deprotonated glutamate is also required in the competent active site, which is formed on binding of the fatty-acyl chain, concomitant with the flipping out of the arginine side chain, as seen in the 1hno apo structure (Fig. 6*b*; in which case this arginine side chain is flipped out). In the latter structure the Asn101 side chain has rearranged somewhat and consequently the Asn101–Glu158 hydrogen-bond interactions are slightly different compared with the other complexes, such that only the Glu158 OE atom is anchored (Fig. 6*b*). Such anchoring geometry, as also observed in HsECI2 and HsECI1 (Fig. 6*a*), would facilitate proton shuttling by the Glu158 carboxylate moiety between the C2 and C4 atoms. In the competent complexed active site (with the Arg100 side chain pointing outwards), the catalytic glutamate is deprotonated, allowing proton abstraction of the C2 proton (of the 3*E*- or 3*Z*-enoyl-CoA substrate) and subsequent transfer of this proton to C4 (forming the 2*E*-enoyl-CoA product). Finally, product release, possibly facilitated by its new geometry owing to the rearrangement of the double bond, and the subsequent swinging back of the Arg100 side chain inwards regenerates the apo structure ready for the next reaction cycle.

In the inward-bound conformation, the side chain of Arg100 closes off an exit acyl-tail binding tunnel shaped by hydrophobic residues and the Asn101 side chain. In its inward conformation the Arg100 side chain is completely buried, but nevertheless there is only one hydrogen bond to the protein part: a hydrogen bond between Arg100 NE and the side chain of Asn101. In order to test the importance of Arg100 and Asn101 for the catalytic function, three point-mutation variants were made (R100A, N101A and N101S). These point-mutation variants have lower T_m values in CD measurements than ScECI2-wt (Fig. 2), especially N101A and N101S, suggesting that the interactions of Asn101 with Arg100 are important for the structure of the wild-type enzyme. These variants are also much less efficient biocatalysts (Table 4), confirming the importance of the Glu158–Asn101–Arg100 hydrogen-bond network present in the apo structures and the Glu158–Asn101 hydrogen-bond interactions in the competent active site.

3.6. The hydrogen-bond networks at the oxyanion hole

The structures of the complexes identify the mode of binding of the thioester O atom in its oxyanion hole shaped by two NH moieties (Table 5). This oxyanion hole is the most conserved part of the crotonase fold. It is of interest to note that the peptide units of these NH moieties are part of extended hydrogen-bond networks (Fig. 8). Comparisons with other members of the crotonase superfamily confirm that these hydrogen-bond networks are conserved. From bio-computational studies it is predicted that such cooperative hydrogen-bond networks will affect the electrostatic properties of these oxyanion holes (Guo & Salahub, 1998; Wieczorek & Dannenberg, 2003). Recent studies have shown that the electrostatic potential in oxyanion holes can be considerable (Fried *et al.*, 2014). In the crotonase fold, one hydrogen bond (provided by the Gly125-Leu126 peptide NH) is part of the cooperative hydrogen-bond network of helix 3 (Fig. 8). It has been pointed out that the binding of negative charges at the N-terminus of an α-helix is favoured by the helix dipole (Hol *et al.*, 1978; Hol, 1985). The cooperativity of the hydrogen-bond network of the helix (Guo & Salahub, 1998) would enhance these favourable electrostatic interactions of the helix with the negatively charged intermediate. The other hydrogen-bond donor is the Gly69-Ala70 peptide NH of loop 2, which is also part of a hydrogen-bond network (Fig. 8). In each of the analyzed crotonase structures this extended hydrogen-bond network, as described here for ScECI2, is

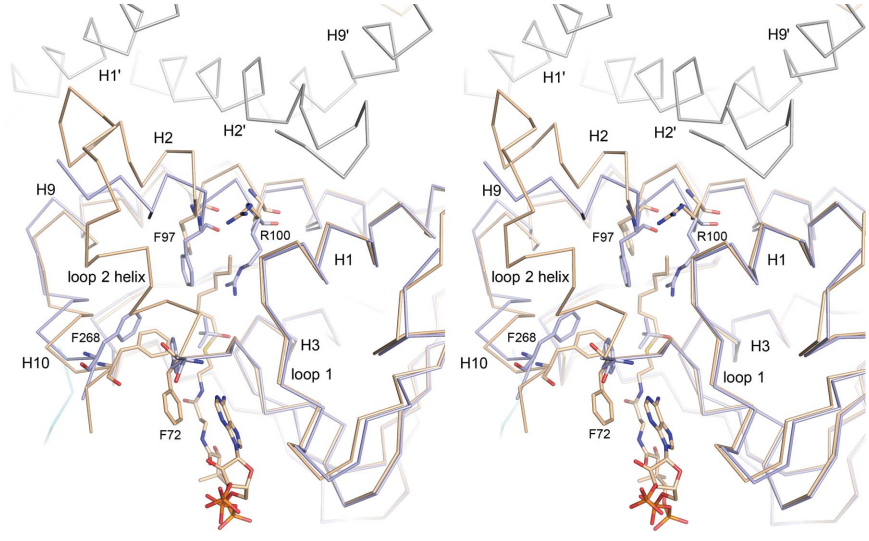

Figure 7
Stereoimage showing the C$^{\alpha}$ traces of the ScECI2-CO8 (tight hexamer; light brown; including octanoyl-CoA) and the ScECI2-SO4 apo (loose hexamer; light blue) structures near the active site. The ScECI2-CO8 crystal structure is a tight hexamer and the key helices for hexamerization (H1′, H2′ and H9′) of chain *C*′ are also shown (same view as in Fig. 4). The inward-pointing Arg100 and Phe72 (covering the adenine ring of octanoyl-CoA), Phe97 (lining the tunnel for the fatty acyl-CoA tail) as well as Phe268 (hydrophobic cluster; H10) are also shown for both structures.

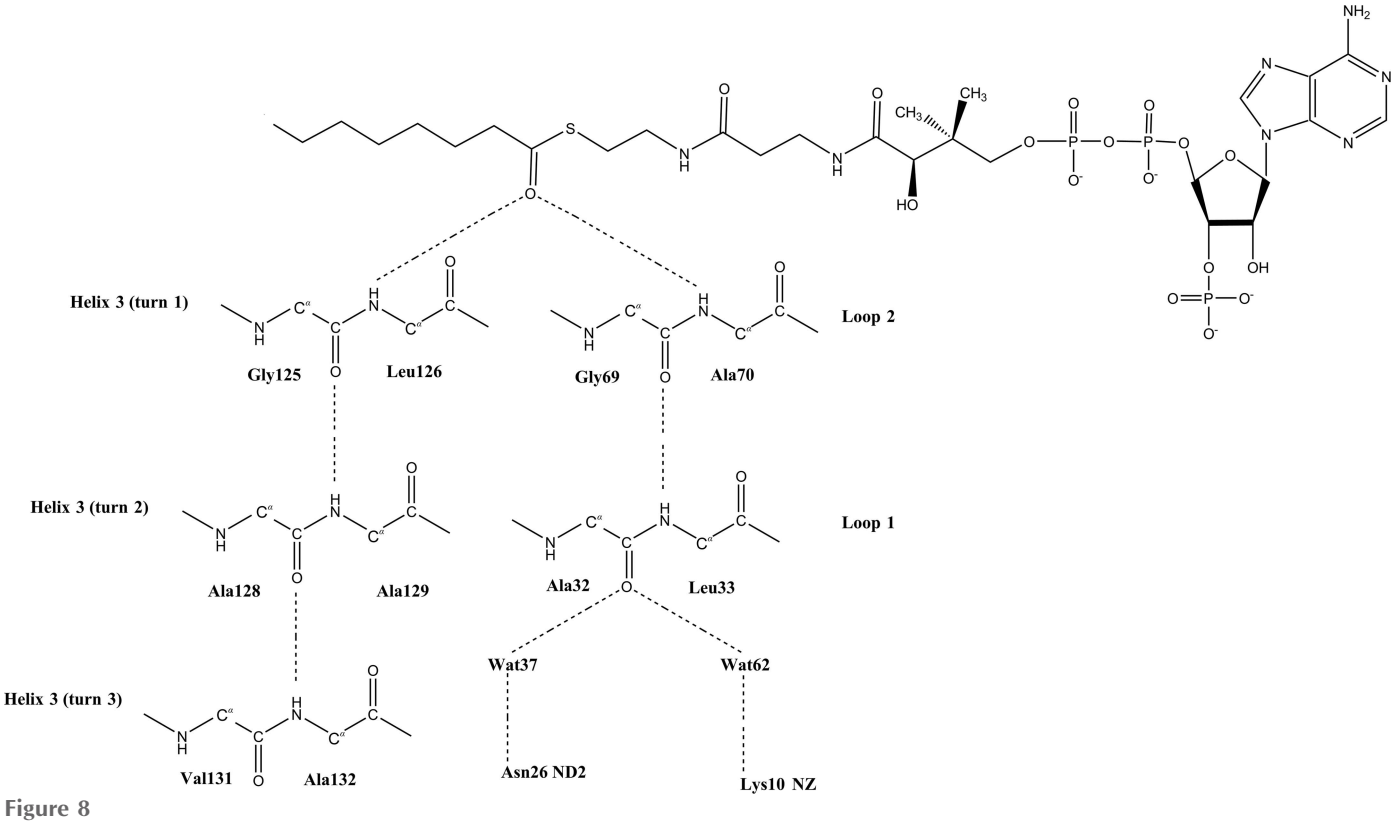

Figure 8
The hydrogen-bond networks of the oxyanion-hole peptide groups. The thioester O atom is hydrogen-bonded to Leu126 N and Ala70 N. The extended hydrogen-bond networks of the peptidyl O atoms of the respective peptide units are shown.

conserved. The cooperative hydrogen bonds of the latter hydrogen-bond network would also provide a significant stabilization of the binding of the negatively charged transition state in the oxyanion hole, like the hydrogen-bond network of helix 3. The Gly69-Ala70 peptide unit is flanked by the Ser68-Gly69 and Ala70-Asp71 peptide units and the peptide O atoms of Ser68 and Ala70 are hydrogen-bonded to the adenine NH_2 moiety (Table 5). There are no structural rearrangements in the Ser68–Asp71 region of loop 2 on binding of the adenine moiety. It will be interesting to investigate whether the hydrogen-bond interactions of the adenine NH_2 moiety further increase the power of the oxyanion hole generated by Ala70 N positioned in the middle of this rigid fragment of loop 2.

4. Concluding remarks

Two different crystal forms of native ScECI2 have been observed, with either a tight hexameric or a trimeric (loose hexameric) assembly. In both crystal forms the Arg100 side chain can point inwards (blocking the binding of the acyl chain) or outwards. The trimeric form has only been obtained at low pH (pH 5.5 and 5.6) and the hexameric form at higher pH (pH 6.5 and 7.0). Solution experiments (Mursula *et al.*, 2004) show that in solution a hexameric assembly is observed at both pHs. At pH 7.2 the enzyme activity is 20-fold higher than at pH 5.6 (Mursula, 2002; the optimum pH is at pH 9.0), suggesting that the hexameric form is a catalytically functional enzyme, which then, with the Arg100 side chain pointing outwards, binds and interconverts the enoyl-CoA substrates. Although the structure of the enzyme–substrate complex is not available, the structural and mutagenesis data show the importance of the Glu158–Asn101–Arg100 hydrogen-bond interactions in the competent complexed and apo structures. In the ScECI2-CO8 structure the acyl chain of octanoyl-CoA is bound in a bent conformation, mimicking the 3*Z* conformation of the 3*Z*-octenoyl-CoA substrate, suggesting that 3*Z*-enoyl-CoA might be a better substrate. It will be interesting to establish whether the catalytic efficiencies for the 3*Z* and 3*E* substrate molecules are the same or different. In the liganded crystal structures (ScECI2-CAA and ScECI2-CO8) the 3′,5′-diphosphate-adenosine part is better bound than the acyl chain. This may be a crystal-packing artefact, but it suggests that the 3′,5′-diphosphate-adenosine part, which interacts with loops 1 and 2 (Fig. 5), functions as an anchor facilitating the binding of the acyl tail in its binding tunnel near the catalytic site. The binding of the adenine moiety also favours the outward-pointing conformation of the Phe72 side chain (being stacked against the adenine moiety).

The helix 10 point-mutation and deletion variants are less active or inactive, respectively, as also observed in the corresponding HsECI2 studies. In these variants loop 2 and helix 10 have adopted different conformations. The side chains of loop 2 (Phe72 and Ile75) and helix 10 (Phe268) contribute to the hydrophobic cluster that interacts with the thioester substrate moiety, and this hydrophobic cluster is disrupted in these two

variants. The disruption of this cluster has been proposed to be responsible for the lower activity or inactivity of these variants, respectively. Loop 2 and helix 10 as well as the hydrophobic cluster are also different in the trimeric (loose hexameric) assembly of ScECI2, also suggesting that the trimer is not a catalytically competent form.

The conservation of the oxyanion-hole geometry in the crotonase superfamily is striking. Also striking are the conserved interactions of the adenine NH2 moiety with loop 2. Loop 2 also provides one of the oxyanion-hole peptide NH hydrogen-bond donors. The other peptide NH hydrogen-bond donor of the oxyanion hole is provided by the N-terminus of helix 3. Careful analysis of this oxyanion-hole geometry shows that each of these peptide NH groups are part of extended hydrogen-bond networks. Further experimental and computational studies are required to probe the importance for catalysis of these hydrogen-bond networks, which are a conserved feature of the crotonase superfamily.

Acknowledgements

We very much appreciate the support of the beamline scientists at EMBL-DESY (P13), ESRF (ID29) and DLS (I04-1) during data collection. We also acknowledge the support of the Academy of Finland (141487) for the *xtalPiMS* project and The Finnish Society of Sciences and Letters (Magnus Ehrnrooth Foundation) for grant support for the ECI2 project. The use of the facilities and expertise of the Biocenter Oulu core facility, a member of Biocenter Finland and Instruct-FI, is also gratefully acknowledged. The research leading to these results received funding from the European Community's Seventh Framework Programme (FP7/2007–2013) under BioStruct-X (grant agreement No. 283570). We thank Dr John Richard for stimulating discussions.

References

Amyes, T. L. & Richard, J. P. (2013). *Biochemistry*, **52**, 2021–2035.
Benning, M. M., Taylor, K. L., Liu, R.-Q., Yang, G., Xiang, H., Wesenberg, G., Dunaway-Mariano, D. & Holden, H. M. (1996). *Biochemistry*, **35**, 8103–8109.
Binstock, J. F. & Schulz, H. (1981). *Methods Enzymol.* **71**, 403–411.
Chen, V. B., Arendall, W. B., Headd, J. J., Keedy, D. A., Immormino, R. M., Kapral, G. J., Murray, L. W., Richardson, J. S. & Richardson, D. C. (2010). *Acta Cryst.* D**66**, 12–21.
Emsley, P. & Cowtan, K. (2004). *Acta Cryst.* D**60**, 2126–2132.
Engel, C. K., Kiema, T. R., Hiltunen, J. K. & Wierenga, R. K. (1998). *J. Mol. Biol.* **275**, 847–859.
Evans, P. R. & Murshudov, G. N. (2013). *Acta Cryst.* D**69**, 1204–1214.
Fried, S. D., Bagchi, S. & Boxer, S. G. (2014). *Science*, **346**, 1510–1514.
Geisbrecht, B. V., Zhang, D., Schulz, H. & Gould, S. J. (1999). *J. Biol. Chem.* **274**, 21797–21803.
Geisbrecht, B. V., Zhu, D., Schulz, K., Nau, K., Morrell, J. C., Geraghty, M., Schulz, H., Erdmann, R. & Gould, S. J. (1998). *J. Biol. Chem.* **273**, 33184–33191.
Guo, H. & Salahub, D. R. (1998). *Angew. Chem. Int. Ed.* **37**, 2985–2990.
Gurvitz, A., Mursula, A. M., Firzinger, A., Hamilton, B., Kilpeläinen, S. H., Hartig, A., Ruis, H., Hiltunen, J. K. & Rottensteiner, H. (1998). *J. Biol. Chem.* **273**, 31366–31374.
Haataja, T. J., Koski, M. K., Hiltunen, J. K. & Glumoff, T. (2011). *Biochem. J.* **435**, 771–781.
Hamed, R. B., Batchelar, E. T., Clifton, I. J. & Schofield, C. J. (2008). *Cell. Mol. Life Sci.* **65**, 2507–2527.
Hamed, R. B., Gomez-Castellanos, J. R., Thalhammer, A., Harding, D., Ducho, C., Claridge, T. D. & Schofield, C. J. (2011). *Nature Chem.* **3**, 365–371.
Hamed, R. B., Henry, L., Gomez-Castellanos, J. R., Asghar, A., Brem, J., Claridge, T. D. & Schofield, C. J. (2013). *Org. Biomol. Chem.* **11**, 8191–8196.
Hamed, R. B., Henry, L., Gomez-Castellanos, J. R., Mecinović, J., Ducho, C., Sorensen, J. L., Claridge, T. D. & Schofield, C. J. (2012). *J. Am. Chem. Soc.* **134**, 471–479.
Hamed, R. B., Mecinović, J., Ducho, C., Claridge, T. D. & Schofield, C. J. (2010). *Chem. Commun.* **46**, 1413–1415.
Hiltunen, J. K., Mursula, A. M., Rottensteiner, H., Wierenga, R. K., Kastaniotis, A. J. & Gurvitz, A. (2003). *FEMS Microbiol. Rev.* **27**, 35–64.
Hiltunen, J. K. & Qin, Y. (2000). *Biochim. Biophys. Acta*, **1484**, 117–128.
Hol, W. G. J. (1985). *Prog. Biophys. Mol. Biol.* **45**, 149–195.
Hol, W. G. J., van Duijnen, P. T. & Berendsen, H. J. C. (1978). *Nature (London)*, **273**, 443–446.
Holden, H. M., Benning, M. M., Haller, T. & Gerlt, J. A. (2001). *Acc. Chem. Res.* **34**, 145–157.
Janssen, U., Fink, T., Lichter, P. & Stoffel, W. (1994). *Genomics*, **23**, 223–228.
Jencks, W. P. (1987). *Cold Spring Harb. Symp. Quant. Biol.* **52**, 65–73.
Kabsch, W. (2010). *Acta Cryst.* D**66**, 125–132.
Kamerlin, S. C. L., Chu, Z. T. & Warshel, A. (2010). *J. Org. Chem.* **75**, 6391–6401.
Kasaragod, P., Schmitz, W., Hiltunen, J. K. & Wierenga, R. K. (2013). *FEBS J.* **280**, 3160–3175.
Kasaragod, P., Venkatesan, R., Kiema, T. R., Hiltunen, J. K. & Wierenga, R. K. (2010). *J. Biol. Chem.* **285**, 24089–24098.
Kilponen, J. M., Palosaari, P. M., Sormunen, R. T., Vihinen, M. & Hiltunen, J. K. (1992). *Prog. Clin. Biol. Res.* **375**, 33–40.
Krissinel, E. & Henrick, K. J. (2007). *J. Mol. Biol.* **372**, 774–797.
Moore, S. A. & Jencks, W. P. (1982). *J. Biol. Chem.* **257**, 10893–10907.
Murshudov, G. N., Skubák, P., Lebedev, A. A., Pannu, N. S., Steiner, R. A., Nicholls, R. A., Winn, M. D., Long, F. & Vagin, A. A. (2011). *Acta Cryst.* D**67**, 355–367.
Mursula, A. M. (2002). PhD thesis. Oulu University, Finland.
Mursula, A. M., Hiltunen, J. K. & Wierenga, R. K. (2004). *FEBS Lett.* **557**, 81–87.
Mursula, A. M., van Aalten, D. M. F., Hiltunen, J. K. & Wierenga, R. K. (2001). *J. Mol. Biol.* **309**, 845–853.
Mursula, A. M., van Aalten, D. M. F., Modis, Y., Hiltunen, J. K. & Wierenga, R. K. (2000). *Acta Cryst.* D**56**, 1020–1023.
Natarajan, A., Schwans, J. P. & Herschlag, D. (2014). *J. Am. Chem. Soc.* **136**, 7643–7654.
Onwukwe, G. U., Kursula, P., Koski, M. K., Schmitz, W. & Wierenga, R. K. (2015). *FEBS J.* **282**, 746–768.
Palosaari, P. M. & Hiltunen, J. K. (1990). *J. Biol. Chem.* **265**, 2446–2449.
Pápai, I., Hamza, A., Pihko, P. M. & Wierenga, R. K. (2011). *Chem. Eur. J.* **17**, 2859–2866.
Partanen, S. T., Novikov, D. K., Popov, A. N., Mursula, A. M., Kalervo Hiltunen, J. & Wierenga, R. K. (2004). *J. Mol. Biol.* **342**, 1197–1208.
Rasmussen, J. T., Börchers, T. & Knudsen, J. (1990). *Biochem. J.* **265**, 849–855.
Sleeman, M. C., Sorensen, J. L., Batchelar, E. T., McDonough, M. A. & Schofield, C. J. (2005). *J. Biol. Chem.* **280**, 34956–34965.
Weeghel, M. van, Ofman, R., Argmann, C. A., Ruiter, J. P., Claessen, N., Oussoren, S. V., Wanders, R. J., Aten, J. & Houten, S. M. (2014). *FASEB J.* **28**, 1365–1374.
Weeghel, M. van, te Brinke, H., van Lenthe, H., Kulik, W., Minkler, P. E., Stoll, M. S., Sass, J. O., Janssen, U., Stoffel, W., Schwab, K. O., Wanders, R. J., Hoppel, C. L. & Houten, S. M. (2012). *FASEB J.* **26**, 4316–4326.

Whitty, A., Fierke, C. A. & Jencks, W. P. (1995). *Biochemistry*, **34**, 11678–11689.
Wieczorek, R. & Dannenberg, J. J. (2003). *J. Am. Chem. Soc.* **125**, 8124–8129.
Winn, M. D. *et al.* (2011). *Acta Cryst.* D**67**, 235–242.
Winter, G. (2010). *J. Appl. Cryst.* **43**, 186–190.
Xiang, H., Luo, L., Taylor, K. L. & Dunaway-Mariano, D. (1999). *Biochemistry*, **38**, 7638–7652.
Zhang, D., Yu, W., Geisbrecht, B. V., Gould, S. J., Sprecher, H. & Schulz, H. (2002). *J. Biol. Chem.* **277**, 9127–9132.